Irreversible chemical steps control intersubunit dynamics during translation

R. Andrew Marshall*, Magdalena Dorywalska†, and Joseph D. Puglisi†‡§

*Department of Chemistry, Stanford University, Stanford, CA 94305-5080; †Department of Structural Biology, Stanford University School of Medicine, Stanford, CA 94305-5126; and ‡Stanford Magnetic Resonance Laboratory, Stanford University School of Medicine, Stanford, CA 94305-5126

Edited by Michael Levitt, Stanford University School of Medicine, Stanford, CA, and approved August 25, 2008 (received for review June 2, 2008)

The ribosome, a two-subunit macromolecular machine, deciphers the genetic code and catalyzes peptide bond formation. Dynamic rotational movement between ribosomal subunits is likely required for efficient and accurate protein synthesis, but direct observation of intersubunit dynamics has been obscured by the repetitive, multistep nature of translation. Here, we report a collection of single-molecule fluorescence resonance energy transfer assays that reveal a ribosomal intersubunit conformational cycle in real time during initiation and the first round of elongation. After subunit joining and delivery of correct aminoacyl-tRNA to the ribosome, peptide bond formation results in a rapid conformational change, consistent with the counterclockwise rotation of the 30S subunit with respect to the 50S subunit implied by prior structural and biochemical studies. Subsequent binding of elongation factor G and GTP hydrolysis results in a clockwise rotation of the 30S subunit relative to the 50S subunit, preparing the ribosome for the next round of tRNA selection and peptide bond formation. The ribosome thus harnesses the free energy of irreversible peptidyl transfer and GTP hydrolysis to surmount activation barriers to large-scale conformational changes during translation. Intersubunit rotation is likely a requirement for the concerted movement of tRNA and mRNA substrates during translocation.

ribosome dynamics | single-molecule FRET | translocation

Translation of the genetic code into proteins by the ribosome requires precise, dynamic interplay between numerous protein and RNA elements. The ribosome, a two-subunit, ribonucleoprotein assembly, coordinates these dynamics to read the genetic code and synthesize proteins (1–3). The large and small ribosomal subunits (50S and 30S, respectively) have three distinct transfer RNA (tRNA) binding sites: A (aminoacyl), P (peptidyl), and E (exit), where messenger RNA (mRNA) is decoded and peptide bonds are formed (4–6). The ribosome works in concert with protein factors, including GTPases whose catalytic activity is modulated by the ribosome and its substrates (7, 8). During translation initiation, the ribosome is assembled at an AUG start codon on an mRNA and charged with fMet-tRNA^{fMet} in the P site. This complex is competent to engage in repetitive cycles of peptide elongation during which aminoacyl-tRNAs are selected at the A site, peptide bonds are formed in the P site, and tRNAs with their associated mRNA codons are translocated from the A and P sites to the P and E sites, respectively (1, 3).

Directional movement of mRNA and tRNA on the ribosome during elongation is likely controlled by dynamic changes in ribosome structure (9). High-resolution structural models suggest that the movement of ribosomal domains is intimately linked to key events during translation (10, 11). Furthermore, cryo-electron microscopy (cryo-EM) of ribosome complexes trapped during elongation has identified two functional ribosome states that are related by rotation of the 30S subunit with respect to the 50S subunit (12, 13). Recent bulk fluorescence measurements of ribosome complexes stalled at various stages during elongation corroborate these findings in solution (14). A ratchet-like mechanism has been proposed to explain the oscillation of the ribosome between these two functional states during translation (12). Yet detailed studies of static ribosome complexes have not revealed how the ribosome transitions between these two states, or how the proposed rotational movements are regulated.

Here, we perform single-molecule fluorescence assays with site-specifically labeled 30S and 50S ribosomal subunits, which permit the real-time observation of initiation and the first round of peptide bond formation by fluorescence resonance energy transfer (FRET) (Fig. 1). Our results establish a temporal correlation of intersubunit dynamics with ligand binding and chemical events during translation.

Experimental Design and Results. To observe intersubunit dynamics during translation via FRET, mutant *Escherichia coli* ribosomes with extended rRNA hairpins were engineered to allow site-specific hybridization of fluorescently labeled oligonucleotides to both 30S and 50S subunits according to reported methodology (15). The 50S subunit was modified at helix 101, which is located at the periphery of the subunit interface within ≈45 Å of a previously reported helix 44 extension on the 30S subunit providing for the observation of FRET between doubly labeled ribosomes [Fig. 1*A* and supporting information (SI) Fig. S1]. These labeling positions are distant (>120 Å) from ribosomal active sites where peptidyl transfer and decoding take place, from known dynamic domains of the individual subunits: the 30S head and 50S L1 and L7/L12 stalks (10, 16–18). After the attachment of fluorescent labels, mutant ribosomes remain fully competent to bind ternary complex and translocate with elongation factor G (EF-G) (Fig. S2*B*). Probes attached in this relatively static region of the ribosome allow observation of global intersubunit dynamics that are uncomplicated by local conformational changes.

Preinitiation complexes (PICs) assembled with Cy3-labeled 30S subunits, a 5′-biotinylated 57-nucleotide mRNA derived from T4 gene 32 mRNA, fMet-tRNA^{fMet}, and initiation factor 2 (IF2) were immobilized on a neutravidin-derivatized quartz surface, as previously described (Fig. 1*B*) (19). Observation of individual ribosomes under constant 532-nm laser illumination during subunit joining and the first round of translation was achieved by stopped-flow delivery at 22° C of Cy5-labeled 50S subunits, ternary complex of EF-Tu/GTP/Phe-tRNA^{Phe}, and EF-G in a background of saturating IF2, fMet-tRNA^{fMet}, and GTP (see *Materials and Methods*).

The transitions from initiation through the first peptide bond formation and translocation are observed directly in our single-molecule (sm) assays. Analysis of smFRET-time traces recorded

Author contributions: R.A.M. and J.D.P. designed research; R.A.M. performed research; R.A.M. and M.D. contributed new reagents/analytic tools; R.A.M. and J.D.P. analyzed data; and R.A.M., M.D., and J.D.P. wrote the paper.

The authors declare no conflict of interest.

This article is a PNAS Direct Submission.

§To whom correspondence should be addressed. E-mail: puglisi@stanford.edu.

This article contains supporting information online at www.pnas.org/cgi/content/full/0805299105/DCSupplemental.

www.pnas.org/cgi/doi/10.1073/pnas.0805299105

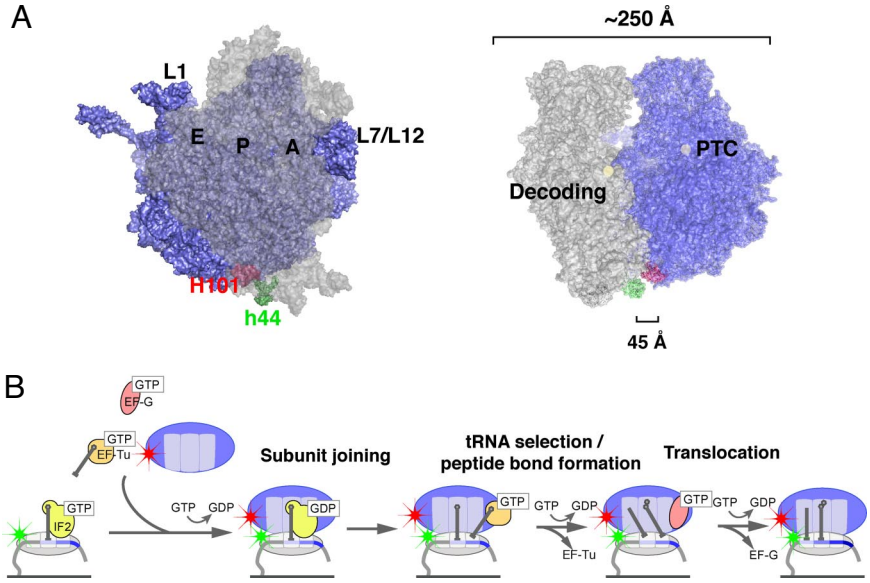

Fig. 1. Experimental design for single-molecule observation of intersubunit FRET. (*A Left*) Surface representation of the 70S ribosome complex from *E. coli* viewed from the solvent side of the 30S subunit (transparent gray) shows the locations of helical extensions engineered into the ribosome. Helix 101 (H101) of the 50S subunit (blue) is labeled in red, and helix 44 of the 30S subunit (h44) is in green. The chosen labeling sites are distant from the dynamic components of the ribosome (L1, L7/L12) and the functional sites (A, P, and E sites). (*Right*) Side view of the 70S ribosome showing the distance between mutation sites (≈45 Å). Both the peptidyltransferase center and decoding center are >120 Å from the labeling sites. (*B*) Schematic representation of the single-molecule fluorescence assays applied here to view translation in real time. Cy5-labeled 50S subunits (blue with red star) and elongation factors EF-Tu (orange) and EF-G (pink) are stopped-flow delivered to Cy3-labeled 30S preinitiation complexes (gray with green star) formed with IF2 (yellow), fMet-tRNA^{fMet} (dark gray line), and a biotinylated mRNA (curved line). With this methodology, subunit joining, tRNA selection, and translocation are observed on the surface-immobilized ribosomes.

during the codelivery of 20 nM Cy5–50S, 20 nM ternary complex, and 20 nM EF-G to Cy3–30S PICs reveals three ordered FRET transitions from zero to 0.45, 0.45 to 0.35, and 0.35 to 0.45 (Fig. 2*C*). In the absence of ternary complex and EF-G, a single transition is observed from zero to a steady long-lived 0.45 FRET value (τ = 160.1 s) (Fig. 2*A* and Fig. S3). This first transition represents 30S–50S subunit joining and is blocked during the delivery of 20 nM Cy5–50S in the presence of 125 nM unlabeled MRE 600 30S subunits or by incubation of immobilized Cy3–30S PICs in the presence of 2 μM unlabeled MRE 600 50S subunits before Cy5–50S delivery (data not shown). The observed FRET value of 0.45 with the Cy3-Cy5 donor-acceptor pair is consistent with the interfluorophore distance of 45 Å predicted from high-resolution structures of the *E. coli* ribosome. The apparent first-order rate for Cy5–50S arrival to immobilized Cy3–30S PICs is 0.082 ± 0.022 s^{-1} (Fig. S3*B*), which is an order of magnitude slower than the observed bulk bimolecular rate constant of 140 μM^{-1} s^{-1} for subunit joining in the presence of IF2 at 37°C (20).

Ternary complex binding is responsible for the second observed FRET transition. The codelivery of Cy5–50S subunits and ternary complex in the absence of EF-G results in smFRET traces in which the initial FRET transition on subunit joining is followed only by an irreversible transition from 0.45 to 0.35 FRET (Fig. 2*B*). The magnitude of this decrease in FRET efficiency is consistent with a change in interfluorophore distance of ≈5Å reflective of the counterclockwise rotation of the 30S subunit seen in the conversion of the initiation conformation of the ribosome to the pretranslocation conformation by using cryoEM (12). The rate of subunit joining is unaffected by the presence of ternary complex (0.088 ± 0.02 s^{-1}), and the mean dwell time at 0.45 FRET before transition to 0.35 FRET is 19.5 ± 1.9 s. Ternary complex delivery experiments were validated by observing FRET between elbow-labeled tRNAs as previously described (19, 21). Codelivery of unlabeled 50S and ternary complex of Cy5-labeled Phe-tRNA^{Phe} to unlabeled 30S PICs with Cy3-labeled fMet-tRNA^{fMet} in the P site confirms that surface-initiated 70S complexes are active in peptidyl transfer and hybrid state formation at both 5 and 15 mM Mg^{2+} (Fig. S4). Unlike A- and P-site tRNAs, which show Mg^{2+}-dependent fluctuations between classical and hybrid states on a 100-ms timescale (19, 22), the intersubunit conformation of the ribosome is stable after ternary complex delivery, the kinetics is not strongly affected by Mg^{2+}, and fluctuations to the 0.45 state are not observed (data not shown).

Stable accommodation of tRNA is required for the observed intersubunit conformational transition. Delivery of Cy5–50S and ternary complex in the presence of a near-cognate A-site codon (CUU) completely inhibits the transition from 0.45 to 0.35 FRET without affecting the rate of subunit joining (Fig. S5). Delivery in the presence of 50 μM kirromycin, an antibiotic that inhibits full accommodation of tRNA in the A site, results in a 4-fold suppression of the 0.45 to 0.35 FRET transition frequency (Fig. S5). Kirromycin locks EF-Tu in its GDP-bound state without affecting its GTPase activity, suggesting that the intersubunit conformational change is not linked to the free energy of GTP hydrolysis. Cryo-EM structures show no relative rotation of 30S subunit with respect to 50S subunits when ternary complex selection is stalled with kirromycin (23, 24).

To probe directly the timing of tRNA binding and the intersubunit conformational change, a three-color experiment was performed to monitor intersubunit FRET and A-site tRNA arrival simultaneously. Ternary complex of Phe-tRNA^{Phe} labeled with Cy2, a fluorophore excited at 492 nm and detected at 507 nm was codelivered with Cy5–50S subunits to surface-immobilized Cy3–30S PICs (Fig. 3*A*). Stopped-flow delivery under constant 488- and 532-nm illumination at 15 mM Mg^{2+} reveals anticorrelated fluorescence from Cy3 and Cy5, indicative of intersubunit FRET, and concurrent Cy2 fluorescence, which is observed as both long-lived and transient bursts (Fig. 3*B*). The intersubunit FRET transition from 0.45 to 0.35 observed between Cy3 and Cy5 in these three-color experiments is the same

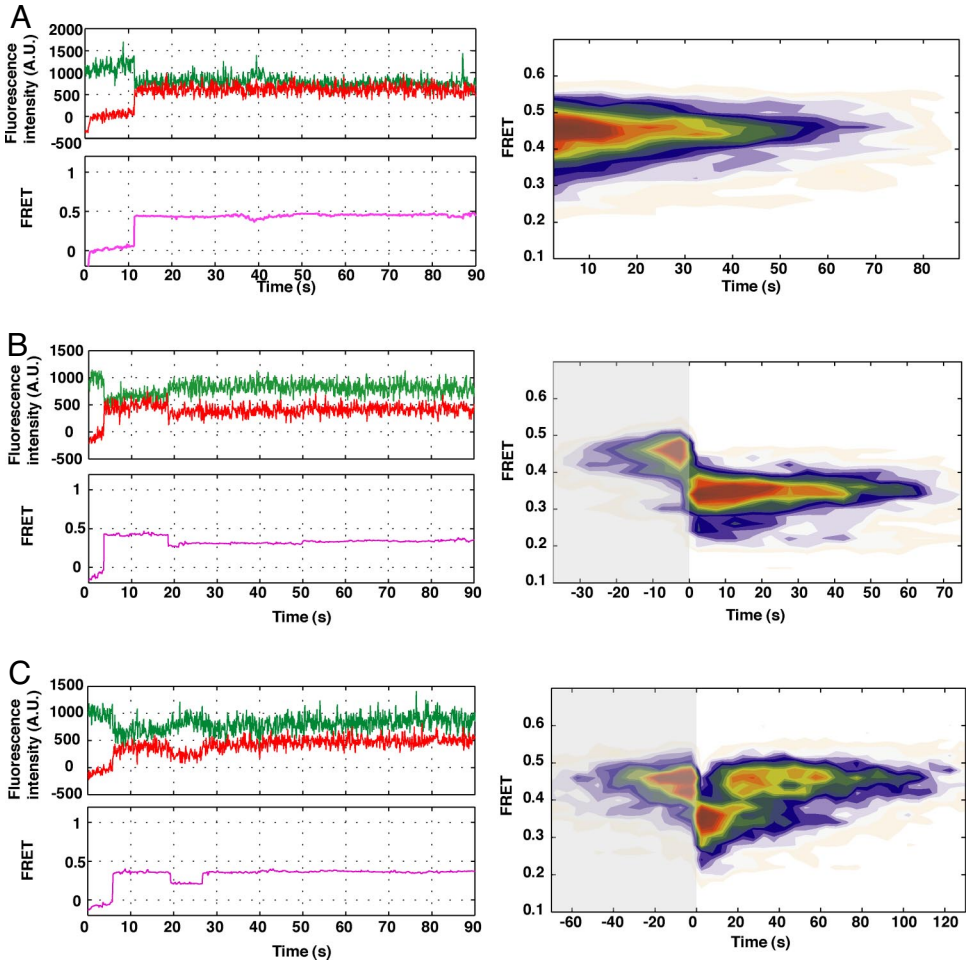

Fig. 2. Representative single-molecule fluorescence and FRET traces. *A* to *C* each show a representative raw fluorescence trace for Cy3 and Cy5 fluorophores during stopped-flow delivery of Cy5-labeled 50S subunits to immobilized Cy3-labeled 30S PICs under a various conditions. (*Left*) Below the raw fluorescence traces are shown the calculated FRET vs. time traces, which have been smoothed >50 frames (5 s) by using a nonlinear filter (see *Materials and Methods*). (*Right*) Contour plots display the overlay of numerous smFRET traces postsynchronized to specific events during the course of observation. (*A*) Delivery of Cy5-labeled 50S; the contour plot is postsynchronized to the first FRET transition (from zero to 0.45 FRET). (*B*) Delivery of Cy5-labeled 50S in the presence of Phe-tRNAPhe/EF-Tu/GTP ternary complex (TC); the contour plot is postsynchronized to the 0.45 to 0.35 FRET transition. Gray shading highlights the region of the trace before this transition. (*C*) Delivery of Cy5-labeled 50S in the presence of TC and EF-G; the contour plot is postsynchronized to the 0.45 to 0.35 FRET transition, and highlighted as in *B*.

as that observed in the presence of unlabeled Phe-tRNA^{Phe}. Furthermore, the rate of subunit joining, and the time between subunit joining and the 0.45 to 0.35 FRET transition are in agreement with previous measurements reported in this work (Table S1). Of the 0.45 to 0.35 FRET transitions, 97% were observed simultaneously with the arrival of Cy2 fluorescence (Fig. S6). For 30S PICs assembled on an mRNA with a near-cognate A-site codon (CUU), intermittent bursts of Cy2 fluorescence were still observed, but intersubunit conformational changes were completely suppressed (data not shown). Cy2 fluorescent bursts that coincide with the intersubunit FRET change are nearly 6-fold longer than those that do not (6.9 ± 1.1 s vs. 1.25 ± 0.1 s) (Table S1). These data further correlate intersubunit conformational change to full accommodation of tRNA at the A site.

Peptidyl transfer is required for the transition from 0.45 to 0.35 FRET. Delivery of Cy5–50S subunits and ternary complex in the presence of 100 μM chloramphenicol, a peptidyl transferase inhibitor, increases the dwell time at 0.45 FRET before the transition to 0.35 FRET by ≈50% (Fig. S7). Moreover, delivery of Cy5–50S subunits in the presence of 250 μM puromycin, a mimic of the 3′ end of aminoacyl-tRNA that can bind to the A site and react with peptidyl-tRNA in the P site, results in a transition from 0 to 0.45 FRET followed by an irreversible transition from 0.45 to 0.35 FRET (Fig. S7), much like the transitions observed during Cy5–50S and ternary complex delivery (Fig. 2*B*). Puromycin does not affect the rate of subunit joining (0.076 ± 0.023 s^{-1}), and the dwell time at 0.45 FRET, 17.5 ± 2.2 s, is consistent with the bimolecular rate for fMet-Puromycin release determined in bulk and at the single-molecule level (19, 25). These results suggest that the energy of peptidyl transfer, and not tRNA accommodation at the A site, is coupled to intersubunit rotation. A similar conformational change was observed in solution by comparing steady-state FRET values for ribosome complexes before and after reaction with puromycin (14). Interestingly, peptide bond formation also allosterically modulates the energetics of mRNA-ribosome interactions as shown by single-molecule force measurements (26).

EF-G is responsible for the third observed intersubunit FRET transition and the preparation of the ribosome for further rounds of translation. As mentioned above, in the presence of ternary complex and EF-G, surface-initiated 70S complexes transit from 0.45 to 0.35 FRET followed by an irreversible transition to 0.45 FRET (Fig. 2*C*). This transition is consistent with relative rotation of subunits observed in cryo-EM structures of pre- and post-translocation 70S complexes (12) and bulk FRET measurements of 70S

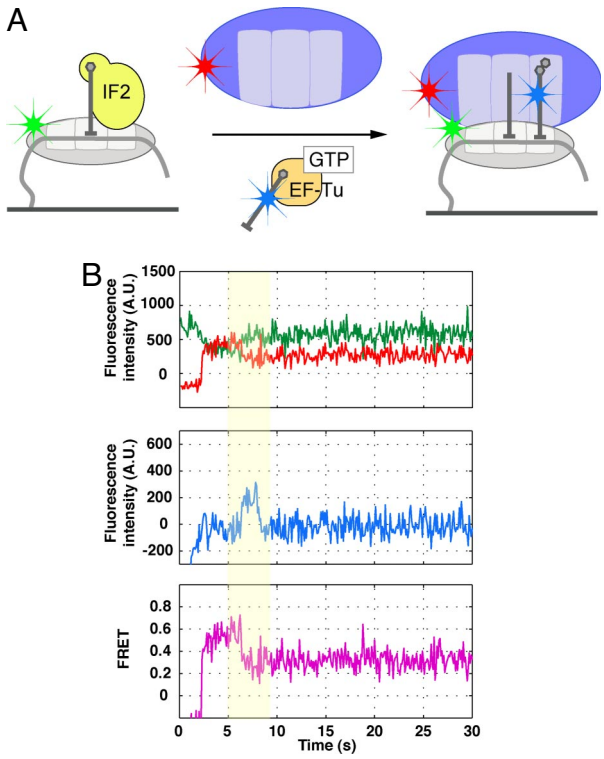

Fig. 3. Three-color experiment demonstrates coincident tRNA binding and intersubunit conformational change. (*A*) A schematic of the three-color experiment. Cy5-labeled 50S subunits and Cy2-labeled TC are codelivered to Cy3-labeled surface-immobilized 30S PICs. Illumination with 488-nm and 532-nm lasers allows for simultaneous observation of intersubunit FRET and Cy2 fluorescence. (*B*) Representative fluorescence and FRET traces from a three-color experiment. (*Top*) Raw Cy3 and Cy5 fluorescence; (*Middle*) Cy2 fluorescence; (*Bottom*) Calculated Cy3-Cy5 FRET. The yellow bar highlights the transition from 0.45 to 0.35 FRET and demonstrates that it occurs simultaneously with the arrival of Cy2 fluorescence.

complexes before and after EF-G-catalyzed translocation (14). Subunit joining is not affected by the presence of ternary complex and EF-G, but the 0.45 to 0.35 FRET transition is slowed ≈2-fold (37.4 ± 3.0 s) in the presence of EF-G (Table S2). EF-G/GTP likely competes with ternary complex for A-site binding. The dwell time at 0.35 FRET before transition to 0.45 FRET is 22.1 ± 1.7 s, which agrees with previously reported bulk measurements of EF-G-dependent translocation rates (1). Inhibition of EF-G release from the posttranslocation 70S complex in the presence of 50 μM antibiotic fusidic acid has little effect on the observed rates of each intersubunit FRET transition (Table S2). This is consistent with the interpretation that the 0.35 to 0.45 FRET transition is triggered by GTP hydrolysis and/or EF-G conformational rearrangement, and not by EF-G dissociation.

Discussion

The confluence of our results with prior structural and biochemical studies support a model in which the ribosome surmounts significant activation barriers to intersubunit conformational changes by using chemical energy provided by each round of translation (Fig. 4). After subunit joining, a transition from 0.45 to 0.35 FRET occurs on formation of the first peptide bond. This transition results from a counterclockwise rotation of the 30S relative to the 50S subunit converting the initiation state of the ribosome to the pretranslocation state, as observed by cryo-EM (12). At room temperature, this transition is essentially irreversible, consistent with a significant activation barrier to intersubunit movement compared with thermal energy in solution and large negative value of the free energy of peptidyl transfer ($\Delta G^\circ = -8$ kcal·mol^{-1}) (27). Peptidyl transfer affects the classical-hybrid state equilibrium between the deacylated tRNA in the P site and peptidyl-tRNA in the A site, influences the affinity of the ribosome for mRNA, and controls GTPase activity of factors (8, 22, 26, 28, 29). However, the structural mechanism for coupling of peptide bond formation to intersubunit conformational change remains unclear. Structural rearrangements in the peptidyl transferase center on peptide bond formation allow for movement of the 3′ end of P-site tRNA to the E site, which may in turn signal rotation of the 30S subunit and lead to disruption of ribosome–mRNA interaction and preparation of the ribosome for translocation (26).

The binding of EF-G to the ribosomal A site and GTP hydrolysis then leads to the directional 5′ to 3′ movement of the ribosome along the mRNA by a single codon. The resultant 0.35 to 0.45 FRET transition is consistent with an irreversible intersubunit reorientation, where the large negative free energy of GTP hydrolysis ($\Delta G^\circ = \approx -10$ kcal·mol^{-1}) (30) is used to facilitate the clockwise rotation of the 30S relative to the 50S subunit, probably mediated by conformational changes of EF-G (12, 14, 31). These events establish the posttranslocation state of the ribosome observed in cryo-EM and bulk FRET studies. In this conformation, the ribosome tightly grips the mRNA and is competent to select the next tRNA at the A site during the subsequent round of translation.

Concurrent with this work, Cornish *et al.* (32) observed spontaneous, reversible intersubunit movement by using smFRET techniques. In their study, *in vitro* reconstituted ribosomes labeled near the L1 stalk with Cy5 on the small-subunit protein S6 and Cy3 on the large-subunit protein L9 were used to show that, at equilibrium, pretranslocation ribosome complexes fluctuate between two conformations. Exhaustive characterization of the intersubunit conformational equilibrium allowed for correlation of ribosomal rotational movement with the classical and hybrid state equilibrium of

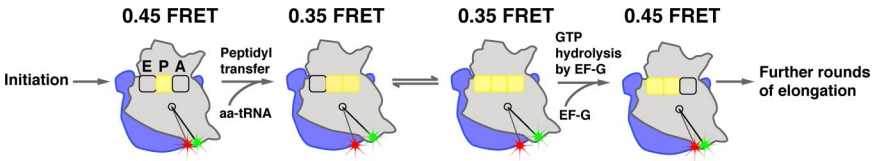

Fig. 4. A model for dynamic intersubunit movement during translation. After subunit joining during initiation, the ribosome (viewed from solvent side of 30S subunit, transparent gray, with 50S in blue) with initiator tRNA in the P site (yellow shading) is competent to enter elongation. This configuration of ribosomal subunits is observed as 0.45 FRET; the relative locations of Cy3 (green star) and Cy5 (red star) dye are highlighted. Delivery of aminoacyl-tRNA (aa-tRNA) to the A site precedes catalysis of the first peptide bond, which occurs rapidly and results in a global counterclockwise rotation of the 30S subunit and a transition to 0.35 FRET. This conformational transition facilitates dynamic movement of A- and P-site tRNAs between classical (A and P sites shaded in yellow) and hybrid states (all three tRNA binding sites shaded in yellow, tRNA in A/P and P/E sites). Additionally, peptide bond formation weakens ribosome–mRNA interactions (26). Subsequent EF-G binding and GTP hydrolysis prompt the directional movement of tRNAs through the ribosome and the ribosome along the mRNA to the P and E sites (yellow shading). These movements are coupled with a clockwise rotation of the 30S subunit with respect to the 50S subunit, which reestablishes the postinitiation conformation of the ribosome (0.45 FRET), and prepares the ribosome for further rounds of translation.

tRNA on the ribosome. From this, a model in which thermally driven intersubunit rotation is coupled to movement of the 3′ ends of tRNA and biased by the action of EF-G was proposed (14, 32). Our results suggest that thermal energy alone is not sufficient to surmount the barrier to intersubunit rotation and that tRNA fluctuations between classical and hybrid states are uncoupled from intersubunit dynamics. It is possible that because of their the proximity the mobile L1 stalk, the ribosome labeling sites chosen by Cornish *et al.* (32) report directly on the local dynamic features of the ribosomal E site, whereas the labeling sites presented in this work report on global intersubunit motions. In fact, Fei *et al.* (33) observed spontaneous motion of the L1 stalk in pretranslocation ribosomes that correlated with the classical/hybrid tRNA equilibrium similar to the unprompted intersubunit motion reported by Cornish *et al.* (32). The results from these studies along with the work presented here offer a model for translocation in which thermally modulated local conformational dynamics of the ribosome control tRNA movement and chemically driven global intersubunit rotation regulate the movement of the ribosome along mRNA. Furthermore, these observations highlight the complexity of ribosome dynamics and the importance of designing multiple labeling strategies for single-molecule translation studies to obtain a complete view of ribosome mechanism.

The results of this study identify the ribosome as a dynamic motor with two distinct interconverting states that are regulated by irreversible chemical events. The rotational movement of ribosomal subunits likely helps to drive the directional movement of mRNA and tRNA substrates through the ribosomal active sites during the multiple rounds of protein synthesis. These ribosomal conformations may also control 70S complex assembly and disassembly during initiation and termination (34–36). Our results underscore the central role of ribosomal intersubunit dynamics in the mechanism of translation.

Materials and Methods

Ribosome Mutagenesis and Mutant Selection. Hairpin loop extensions were introduced into phylogenetically variable, surface-accessible loops of the *E. coli* 16S and 23S rRNAs (Fig. S1*A*) by using a previously reported site-directed mutagenesis approach (15). Regions of the rrnB rRNA operon-carrying carbenicillin-resistant pKK3535 plasmid (37) flanking the 16S rRNA helix 44 mutation site (nucleotides 1450–1453) and the 23S rRNA helix 101 mutation site (nucleotides 2853–2864) were amplified with complementary 23 nucleotide extensions (Fig. S1*B*), and the resulting products were used as composite templates for amplification of each mutant fragment. The mutant rDNA fragments were then ligated back into the plasmid, transformed into the DH5α strain, and selected by using carbenicillin. Plasmids isolated from viable clones were sequenced and retransformed into the SQ380 strain (S. Quan and C. Squires, unpublished data). This strain lacks all seven rrn operons and expresses its rRNA off the pHKrrnC SacB KmR plasmid, which confers sucrose sensitivity and kanamycin resistance. Loss of the wild-type pHKrrnC SacB KmR in viable carbenicillin-selected SQ380 clones was confirmed by their sensitivity to kanamycin and resistance to sucrose. The observed growth rates of the selected clones demonstrate functionality of mutant rRNA *in vivo* (Fig. S2*A*). Activity of isolated mutant ribosomes after hybridization with fluorescent nucleotides was confirmed *in vitro* by using standard toe-printing assays (Fig. S2*B*). Native gel-mobility shift assays were used to verify the efficiency and specificity of oligonucleotide hybridization to both ribosomal target sites (15).

Preparation of Translation Components. 70S tight-coupled ribosomes were purified from SQ380 cells expressing double-mutant ribosomes following standard protocols (38, 39). 30S and 50S subunits were prepared from dissociated tight-coupled 70S particles by using buffer exchange (7.5 mM to 1 mM Mg^{2+}) and purification by sucrose gradient ultracentrifugation (15–40%).

The IF2α gene was PCR-cloned from the *E. coli* C600 genomic DNA into the pProEX HTb plasmid system and overexpressed in BL21 cells according to standard protocols. The pProEX HT plasmid system introduces a six-histidine (6xHis) affinity tag at the amino terminus of the expressed protein with a Tev-protease cleavage site located between the tag and the protein. Cells were lysed by using French press, and the lysate clarified by centrifugation was loaded onto 5-ml HiTrap Ni^{2+} column (GE Healthcare). Purification of the IF2-containing fractions was completed on size exclusion and anion-exchange columns (Superdex 200 and Q Sepharose Fast Flow, respectively).

Translation factors, EF-Tu, EF-Ts, EF-G, and ribosomal protein S1 were overexpressed and purified according to published protocols (19). fMet-tRNA^{fMet} and Phe-tRNA^{Phe} were charged and purified as described in refs. 40 and 41. Fluorescent labeling of tRNA was performed according to published protocols (19).

A 5′-biotinylated 57-nt mRNA construct derived from T4 gene product 32 mRNA was chemically synthesized (Dharmacon). This construct contains a Shine–Dalgarno sequence (UAAGGA) and encodes the first seven amino acids of gp32. 3′-Amino-functionalized DNA oligonucleotides complementary to the hairpin extensions introduced in the 16S and 23S rRNAs were synthesized by IDT and labeled with Cy3- and Cy5-NHS ester derivatives (Amersham Biosciences) according to manufacturer's recommendations.

Real-Time Observation of Translation on Surface-Immobilized Ribosomes. All experiments and preparations were performed in a Tris-based polymix buffer at 5 mM Mg^{2+} without reducing agents at room temperature (≈19°C) unless otherwise mentioned (19). Cy3-labeled 30S preinitiation complexes were prepared and immobilized via the 5′-biotinylated T4 gene product 32-derived mRNA. Purified 30S and 50S ribosomal subunits (final concentration = 1 μM) were mixed in 1:1 stoichiometry with 3′ dye-labeled oligonucleotides specific for hairpin inserts in each subunit and incubated at 37°C for 10 min and then at 30°C for 20 min. Cy3-labeled 30S subunits at 0.5 μM were then incubated at 37°C for 5 min with equimolar ribosomal protein S1 to ensure the homogeneity of purified 30S subunits. 30S preinitiation complexes were formed immediately before single-molecule experiments by incubating Cy3–30S subunits plus S1 (0.25 μM) with 1 μM IF2, 5′-biotinylated mRNA construct, and fMet-tRNA^{fMet} in the presence of 4 mM GTP at 37°C for 5 min. 30S complexes were serially diluted to ≈150 pM in polymix buffer containing 1 μM IF2 and fMet-tRNA^{fMet}, and 4 mM GTP, and then immobilized on a Neutravidin-derivatized quartz slide according to reported protocols (19). Unbound complexes were washed from the slide with an oxygen-scavenged polymix solution containing 1 μM IF2 and fMet- tRNA^{fMet}, 4 mM GTP, 1 mM Trolox, 2.5 mM 3,4-dihydroxybenzoic acid (PCA), and 250 nM protocatechuate dioxygenase (PCD) (42). Real-time observation of 50S subunit joining and the first round of translation was performed by the stopped-flow codelivery of 50 μl of a solution containing Cy5-labeled 50S subunits, ternary complex of EF-Tu, GTP, and Phe-tRNA^{Phe}, prepared according to published protocols (19), and EF-G in a background of 1 μM IF2 and fMet-tRNA^{fMet}, 4 mM GTP, 1 mM Trolox, 2.5 mM PCA, and 250 nM PCD. All experiments were performed as such except for the codelivery of Cy5–50S and ternary complex in the presence of 50 μM kirromycin. In this experiment, equal volumes of a 2× concentrated solution of Cy5–50S and ternary complex delivery solution were rapidly mixed with an oxygen-scavenged solution of 100 μM kirromycin immediately before surface delivery to minimize kirromycin-facilitated GTP hydrolysis by EF-Tu.

All single-molecule fluorescence experiments were performed by using an in-house built, prism-based total internal reflection instrument described in ref. 42. Cy2 and Cy3 fluorophores were excited with 488 nm (320 W/cm^2) and 532 nm (1 kW/cm^2) beams, respectively. Single ribosomes were picked and fluorescence intensity trajectories were recorded postacquisition by using MetaMorph imaging software (Molecular Devices). Analysis of fluorescence intensity trajectories was performed by using MATLAB. Baseline correction of raw fluorescence traces, and Cy2 and Cy3 signal bleedthrough into Cy3 and Cy5 were corrected on a trace-by-trace basis. To increase signal to noise in smFRET trajectories, a nonlinear filter, first described by Chung and Kennedy (43) and recently applied to smFRET analysis by Haran (44), was applied to raw fluorescence traces. Thresholds were then applied allowing for the segregation of states and kinetic analysis of transitions observed in smFRET traces.

ACKNOWLEDGMENTS. We thank C. Squires for providing the SQ380 strain, N. Heredia and D. Maar for cloning of IF2α, C. Aitken, S. Bacallado, and A. Petrov for their assistance with data processing tools, and S. McKenna for critical reading of the manuscript. M.D. was supported by a Howard Hughes Medical Institute Predoctoral Fellowship. This work was supported by National Institutes of Health Grant GM51266.

1. Wintermeyer W. *et al.* (2004) Mechanisms of elongation on the ribosome: Dynamics of a macromolecular machine. *Biochem Soc Trans* 32:733–737.
2. Yonath A (2005) Antibiotics targeting ribosomes: Resistance, selectivity, synergism and cellular regulation. *Annu Rev Biochem* 74:649–679.
3. Steitz TA (2008) A structural understanding of the dynamic ribosome machine. *Nat Rev Mol Cell Biol* 9:242–253.
4. Yusupov MM, *et al.* (2001) Crystal structure of the ribosome at 5.5 Å resolution. *Science* 292:883–896.

5. Selmer M, *et al.* (2006) Structure of the 70S ribosome complexed with mRNA and tRNA. *Science* 313:1935–1942.
6. Korostelev A, Trakhanov S, Laurberg M, Noller HF (2006) Crystal structure of a 70S ribosome-tRNA complex reveals functional interactions and rearrangements. *Cell* 126:1065–1077.
7. Rodnina MV, *et al.* (2000) GTPase mechanisms and functions of translation factors on the ribosome. *Biol Chem* 381:377–387.
8. Zavialov AV, Ehrenberg M (2003) Peptidyl-tRNA regulates the GTPase activity of translation factors. *Cell* 114:113–122.
9. Horan LH, Noller HF (2007) Intersubunit movement is required for ribosomal translocation. *Proc Natl Acad Sci USA* 104:4881–4885.
10. Ogle JM, *et al.* (2001) Recognition of cognate transfer RNA by the 30S ribosomal subunit. *Science* 292:897–902.
11. Schuwirth BS, *et al.* (2005) Structures of the bacterial ribosome at 3.5 Å resolution. *Science* 310:827–834.
12. Frank J, Agrawal RK (2000) A ratchet-like intersubunit reorganization of the ribosome during translocation. *Nature* 406:318–322.
13. Valle M, *et al.* (2003) Locking and unlocking of ribosomal motions. *Cell* 114:123–134.
14. Ermolenko DN, *et al.* (2007) Observation of intersubunit movement of the ribosome in solution using FRET. *J Mol Biol* 370:530–540.
15. Dorywalska M, *et al.* (2005) Site-specific labeling of the ribosome for single-molecule spectroscopy. *Nucleic Acids Res* 33:182–189.
16. Stark H, Rodnina MV, Wieden HJ, van Heel M, Wintermeyer W (2000) Large scale movement of elongation factor G and extensive conformational change of the ribosome during translocation. *Cell* 100:301–309.
17. Agrawal RK, Heagle AB, Penczek P, Grassucci RA, Frank J (1999) EF-G-dependent GTP hydrolysis induces translocation accompanied by large conformational changes in the 70S ribosome. *Nat Struct Biol* 6:643–647.
18. Harms J, *et al.* (2001) High resolution structure of the large ribosomal subunit from a mesophilic eubacterium. *Cell* 107:679–688.
19. Blanchard SC, Kim HD, Gonzalez RL, Puglisi JD, Chu S (2004) tRNA dynamics on the ribosome during translation. *Proc Natl Acad Sci USA* 101:12893–12898.
20. Antoun A, Pavlov MY, Lovmar M, Ehrenberg M (2006) How initiation factors tune the rate of initiation of protein synthesis in bacteria. *EMBO J* 25:2539–2550.
21. Blanchard SC, Gonzalez RL, Kim HD, Chu S, Puglisi JD (2004) tRNA selection and kinetic proofreading in translation. *Nat Struct Mol Biol* 11:1008–1014.
22. Kim HD, Puglisi JD, Chu S (2007) Fluctuations of transfer RNAs between classical and hybrid states. *Biophys J* 93:3575–3582.
23. Valle M, *et al.* (2002) Cryo-EM reveals an active role for aminoacyl-tRNA in the accommodation process. *EMBO J* 21:3557–3567.
24. Stark H, *et al.* (2002) Ribosome interactions of aminoacyl-tRNA and elongation factor Tu in the codon-recognition complex. *Nat Struct Mol Biol* 9:849–854.
25. Semenkov YP, Rodnina MV, Wintermeyer W (2000) Energetic contribution of tRNA hybrid state formation to translocation catalysis on the ribosome. *Nat Struct Mol Biol* 7:1027–1031.
26. Uemura S, *et al.* (2007) Peptide bond formation destabilizes Shine-Dalgarno interaction on the ribosome. *Nature* 446:454–457.
27. Trobro S, Aqvist J (2005) Mechanism of peptide bond synthesis on the ribosome. *Proc Natl Acad Sci USA* 102:12395–12400.
28. Sharma D, Southworth DR, Green R (2004) EF-G-independent reactivity of a pre-translocation-state ribosome complex with the aminoacyl tRNA substrate puromycin supports an intermediate (hybrid) state of tRNA binding. *RNA* 10:102–113.
29. Munro JB, Altman RB, O'Connor N, Blanchard SC (2007) Identification of two distinct hybrid state intermediates on the ribosome. *Mol Cell* 25:505–517.
30. Rutthard H, Banerjee A, Makinen MW (2001) Mg^{2+} is not catalytically required in the intrinsic and kirromycin-stimulated GTPase action of Thermus thermophilus EF-Tu. *J Biol Chem* 276:18728–18733.
31. Savelsbergh A, *et al.* (2003) An elongation factor G-induced ribosome rearrangement precedes tRNA-mRNA translocation. *Mol Cell* 11:1517–1523.
32. Cornish PV, Ermolenko DN, Noller HF, Ha T (2008) Spontaneous intersubunit rotation in single ribosomes. *Mol Cell* 30:578–588.
33. Fei J, Kosuri P, MacDougall DD, Gonzalez RL (2008) Coupling of ribosomal L1 stalk and tRNA dynamics during translation elongation. *Mol Cell* 30:348–359.
34. Myasnikov AG, *et al.* (2005) Conformational transition of initiation factor 2 from the GTP- to GDP-bound state visualized on the ribosome. *Nat Struct Mol Biol* 12:1145–1149.
35. Allen GS, Zavialov A, Gursky R, Ehrenberg M, Frank J (2005) The cryo-EM structure of a translation initiation complex from *Escherichia coli*. *Cell* 121:703–712.
36. Gao H, *et al.* (2007) RF3 induces ribosomal conformational changes responsible for dissociation of class I release factors. *Cell* 129:929–941.
37. Brosius J, *et al.* (1981) Construction and fine mapping of recombinant plasmids containing the rrnB ribosomal RNA operon of *E coli*. *Plasmid* 6:112–118.
38. Powers T, Noller HF (1991) A functional pseudoknot in 16S ribosomal RNA. *EMBO J* 10:2203–2214.
39. Robertson JM, Wintermeyer W (1981) Effect of translocation on topology and conformation of anticodon and D loops of $tRNA^{Phe}$. *J Mol Biol* 151:57–79.
40. Carbon J, David H (1968) Studies on the thionucleotides in transfer ribonucleic acid. Addition of N-ethylmaleimide and formation of mixed disulfides with thiol compounds. *Biochemistry (Mosc)* 7:3851–3858.
41. Schmitt E, Blanquet S, Mechulam Y (1999) Crystallization and preliminary X-ray analysis of *Escherichia coli* methionyl-$tRNA^{fMet}$ formyltransferase complexed with formyl-methionyl-$tRNA^{fMet}$. *Acta Crystallogr D Biol Crystallogr* 55:332–334.
42. Aitken CE, Marshall RA, Puglisi JD (2008) An oxygen scavenging system for improvement of dye stability in single-molecule fluorescence experiments. *Biophys J* 94:1826–1835.
43. Chung SH, Kennedy RA (1991) Forward-backward non-linear filtering technique for extracting small biological signals from noise. *J Neurosci Methods* 40:71–86.
44. Haran G (2004) Noise reduction in single-molecule fluorescence trajectories of folding proteins. *Chem Phys* 307:137–145.